International Journal for Housing Science and Its Applications
Publish August 10, 2025. Volume 46, Issue 4 Pages 141-153

https://doi.org/10.70517/ijhsa46411

Study on the construction of a risk prediction model for freezing and thawing disaster of high-speed railroad roadbed on the Qinghai-Tibet Plateau

Xue Wang[1,*], Xing Wang[1], Jintao Jiang[1] and Bin Zhao[1]
[1] School of Civil Engineering and Water Resources, Qinghai University, Xining, Qinghai, 810016, China
Corresponding authors: (e-mail: hebeiwangxue1@163.com).

Abstract The high-speed railroad on the Qinghai-Tibetan Plateau is located in the highest altitude region in the world, and the permafrost roadbed has been subjected to freeze-thaw cycles for a long time, which leads to disasters such as freezing and thawing of the roadbed, and threatens the safety of railroad operation. In this study, a risk prediction model of freezing and thawing disaster on the roadbed of the Qinghai-Tibet Plateau High-speed Railway is constructed to provide technical support for ensuring the safety of railroad operation in high-altitude areas. The study firstly clarifies the definition and classification of freeze-thaw disaster, which is divided into five types based on the freeze-thaw mechanism: cold weathering-gravity freeze-thaw disaster, freeze-thaw creep-gravity freeze-thaw disaster, freeze-thaw frost cracking disaster, thawing and sinking freeze-thaw disaster, and freezing and sliding disaster. By combining wavelet decomposition, ARIMA and BP neural network methods, a high-precision prediction model was established to assess the temperature change of roadbed and the risk of freeze-thaw hazard. The study collected 685 sets of data for model training and testing, and the results showed that the correlation coefficients R^2 of the training and testing data reached 0.98 and 0.97, respectively, and the percentage of error less than 1% accounted for 90% of the total data. The results applied to the Totuohe and Nagqu station areas on the Tibetan Plateau show that the predicted value of the roadbed surface thaw index in 2020 in the Totuohe area is 1715°C·d, the freezing index is -2024°C·d, and the thaw ratio is 0.8473, which is an increase of more than 7% compared with that in 2000; the predicted value of the thaw ratio in the Nagqu area reaches 1.7768, up more than 10% compared with 2000, indicating that the frozen soil of the roadbed in this region is developing toward thawing, and corresponding protective measures need to be taken to cope with the potential risk of freeze-thaw disaster.

Index Terms Qinghai-Tibetan Plateau, High-speed railroad, Freeze-thaw disaster of roadbed, Wavelet decomposition, ARIMA model, Risk prediction

I. Introduction

The high-speed railroad on the Qinghai-Tibetan Plateau is one of the world's highest elevations and harshest climatic conditions, which includes a large permafrost section [1], [2]. Permafrost roadbed is an important part of the construction of the Qinghai-Tibet Railway. Due to the low winter temperature and high summer temperature in the seasonal permafrost zone, the soil body is in the process of freeze-thaw cycle all year round, which leads to a great difference in structural stresses of this type of soil body in different seasons [3]-[6]. Its reliability plays a crucial role in the safety and stability of railroad operation [7]. However, the susceptibility of permafrost roadbeds to freezing and thawing under the influence of factors such as climate and temperature has led to a series of freeze-thaw disasters [8], [9].

Freezing and thawing disaster is a disease caused by freezing and expansion of soil in the freezing process. As the water in the soil in the freezing process can be migrated to the frozen peak surface, and constantly frozen precipitation of ice, water into ice, the volume increases, so that the relative displacement of soil particles and the occurrence of frost heave, high-speed railroad roadbed was lifted, that is, resulting in frost heave of the soil [10], [11]. When the soil freezes, the transfer of water to the frozen surface also occurs, which increases the amount of frost heave of the soil, and when it melts, it causes the soil to sink violently [12]. The factors affecting frost damage such as frost heave and subsidence in roadbeds are complex, but they can be mainly summarized into four elements: temperature, soil, water and force [13]. Of the four elements, temperature and pressure changes are exogenous, while soil and water are endogenous, and all four elements are present in the freezing process of buildings [14], [15]. Among them, it is worth mentioning that the water in the soil of roadbed is a decisive factor in the formation of roadbed frost damage [16]. And the freezing and thawing disaster of the roadbed of high-speed

railroad can have a great impact on the operation of the railroad, even permanent damage [17], [18]. Therefore, in order to ensure the safety and reliability of railroad transportation, it is of great significance to construct the risk prediction model of freezing and thawing disaster of high-speed railroad roadbed [19], [20].

The high-speed railroad on the Qinghai-Tibet Plateau is one of the railroads with the highest altitude and the most severe climatic conditions in the world, which includes a large permafrost section. Permafrost roadbed is an important part in the construction of Qinghai-Tibet Railway. Due to the seasonal permafrost zone with low temperature in winter and high temperature in summer, the soil body is in the process of freezing and thawing cycle all the year round, which leads to a great difference of structural force of this type of soil body in different seasons. The reliability of permafrost roadbeds plays a crucial role in the safety and stability of railroad operation. However, the susceptibility of permafrost roadbeds to freezing and thawing under the influence of factors such as climate and temperature has led to a series of freeze-thaw disasters. Freeze-thaw hazard is a disease caused by freezing and swelling of the soil during the freezing process. As the water in the soil in the freezing process can migrate to the frozen peak surface and constantly frozen precipitation of ice, water into ice, volume increase, so that the relative displacement of soil particles and the occurrence of frost heave, high-speed railroad roadbed was lifted, that is, resulting in the freezing and thawing of the soil. When the soil freezes, water is also transferred to the freezing surface, which increases the amount of freezing and expansion of the soil, and when it melts, it makes the soil sink drastically. Roadbed produced frost heave, subsidence and other frost damage to the influence of factors is very complex, but can be summarized as temperature, soil quality, moisture and pressure four elements. Of the four elements, changes in temperature and pressure are exogenous, while soil and water are endogenous, and all four elements are present in the process of frost damage to buildings. Among them, it is worth mentioning that the moisture in the soil of roadbed is the decisive factor for the formation of roadbed frost damage. And the freezing and thawing disaster of the roadbed of high-speed railroad can have a great impact on the operation of the railroad, and even permanent damage. Therefore, in order to ensure the safety and reliability of railroad transportation, it is of great significance to construct a risk prediction model of freezing and thawing disaster of high-speed railroad roadbed.

In this study, firstly, the definition and classification of freeze-thaw disaster are discussed in depth, and the scientific classification system of freeze-thaw disaster is established from the mechanism of freeze-thaw action; secondly, the freeze-thaw disaster risk prediction model based on wavelet decomposition, ARIMA model and BP neural network is constructed to realize the high-precision prediction of the temperature change of the roadbed; thirdly, the meteorological and roadbed temperature data of the Tibetan Plateau region are collected, and the model is trained and verified; finally, the model is modified and the prediction model is tested; and lastly, the model is modified and the prediction model is tested. Finally, the model is applied to typical areas along the high-speed railroad on the Tibetan Plateau to predict the future changes in roadbed temperature and freeze-thaw index, assess the risk of freeze-thaw disaster, and provide a scientific basis for the design of railroad roadbed engineering and disaster prevention and mitigation in high-altitude areas. By systematically studying the formation mechanism and prediction method of freeze-thaw disaster, this paper will provide technical support for the safe construction and operation and maintenance of high-speed railroad roadbed projects on the Qinghai-Tibet Plateau.

II. Railway roadbed freeze-thaw disaster risk prediction model

II. A. Definition of freeze-thaw hazard

At present, in various disaster science works, the concept of "freeze-thaw disaster" has not been introduced. Instead, it is described as a type of geological disaster in the form of "special land quality disaster - permafrost disaster" [21]. However, this classification is not scientific enough.

All disasters are the result of the interaction of various roles in nature, in general, by a certain role in the main role, and by the main role of the role of factors determine the type of disaster. For example, tectonics is caused by internal geological forces, and flooding is caused by heavy rainfall (which can be regarded as an external geological force). These various geological internal and external forces are the main power mechanism to create the earth's geomorphology in the earth's stratigraphic system. The earth's own power to regulate the process, generally with intense or slow geological action and appear, when this action and human activities, may produce disaster. In the permafrost area, there are various kinds of freeze-thaw geomorphology formation and status quo, which is called permafrost geomorphology geological process and phenomenon in geology, and generally also known as freezing edge effect and form. Freezing edge refers to a series of processes and accompanying geomorphological phenomena such as migration of water, formation and melting of ice, deformation and displacement of rock and soil, and modification of sediments, which are caused by the freezing of water in rock and soil and the stress generated by the change of temperature and humidity under the negative temperature conditions in the cold climatic environment. At present, most researchers at home and abroad believe that the

freeze-thaw effect is of general significance in the process of ice margin formation, which is the basic process of ice margin effect. There is no need to distinguish between freeze-thaw and ice-marginal action, which are considered to be the same concept in the formation of freeze-thaw disasters. In this study, we believe that the freeze-thaw effect is a universal effect in the process of freeze-thaw disaster formation, and it is an indispensable role in the formation of freeze-thaw disaster (but not necessarily the main force).

II. B.Analysis of the dynamics of freeze-thaw hazards and their classification

II. B. 1) Classification of freeze-thaw action

Geoscience recognizes that the Earth's landforms are the result of various geological internal and external forces. In the case of landforms in cold regions, many experts consider the freezing edge (freezing and thawing) effect to be the main geological force in the formation of landforms in cold regions. It can be assumed that the earth's disasters are also caused by geologic effects, and that they are the stronger ones among the geologic effects. Geological forcing can be considered as a component of the dynamic mechanism of disasters or as a transformation of it. Now, the freeze-thaw action and its classification in geomorphology are introduced into the study of freeze-thaw disasters in order to analyze the dynamic mechanism in freeze-thaw disasters. In geomorphology, freeze-edge (freeze-thaw) actions are categorized as follows.

(1) Weathering - gravity: they are weathering and snow erosion cold freezing weathering, the latter because of the water involved in the full, to help its destructive effect is stronger than the former.

(2) freezing and thawing creep flow - gravity: refers to the frozen soil due to various reasons after thawing, the soil water content increases, more than the plastic limit of the soil, the formation of creep flow, and under the action of gravity, the role of the flow process.

(3) Freezing and thawing sorting: after thawing of permafrost, the original structure of the soil will be reorganized due to the difference in the capacity of each part of the soil.

(4) Freezing and cracking

(5) Thermal thawing effect

(6) Freezing hysteresis and slip promotion effect, it refers to: freezing to make the slope body groundwater enrichment, seasonal freezing and thawing to reduce the strength of the slope broken soil body (this effect in the engineering life of the role, in addition, freezing and thawing and soil genesis relationship, freezing and thawing in the formation of the role of soil and soil formation of the freezing and thawing effect on the effect of the yet to be thought), freezing and thawing increase the static and dynamic pressure of water in the slope area.

II. B. 2) Classification by type of freeze-thaw action

Freeze-thaw disasters are categorized in different ways from different perspectives of research. Because of disciplines and history, it is often seen that freeze-thaw disaster classification method is divided by the type of affected project, which is divided into urban freeze-thaw disaster, transportation engineering freeze-thaw disaster, mining engineering freeze-thaw disaster, water conservancy engineering freeze-thaw disaster and so on, this classification is the result of research with different disciplines separately. Classification according to freeze-thaw mechanism is more conducive to the study of freeze-thaw disaster. Freeze-thaw disasters are categorized according to the following methods.

The classification of the types of freeze-thaw disasters should be adapted to the classification of freeze-thaw action, and the fundamental principle of its role in the formation of the disaster should be taken as the fundamental principle, and a comprehensive analysis should be carried out to determine it in conjunction with engineering practice. The method of categorizing freeze-thaw disaster according to the mechanism of action helps to make scientific forecast for different categories of freeze-thaw disaster. According to the above ideas, freeze-thaw disaster can be divided into the following types: cold weathering - gravity freeze-thaw disaster, freeze-thaw creep - gravity action freeze-thaw disaster, freeze-thaw frost cracking disaster, thawing and sinking freeze-thaw disaster, freezing and sliding disaster, according to the type of freeze-thaw action to classify the type of freeze-thaw disaster, freeze-thaw disaster causes in-depth study, is conducive to the study of freeze-thaw disaster.

II. C.Wavelet Decomposition Based Risk Prediction Model for Freeze-Thaw Disasters

For a certain temperature time series $f(x)$, the wavelet transform enables a multilevel decomposition and reconstruction of this time series, and then the individual sequences are studied separately [22]. Assuming that φ_{nk}, ψ_{nk} are orthogonal wavelet bases in L^2, then for any $f \in L^2$, $f(x)$ can be expanded as:

$$f(x) = \sum_k c_k^o \varphi_{ok} \tag{1}$$

The above equation can be decomposed and reconstructed using the Mallat algorithm, which is a decomposition of $f(t)$ according to different frequency channels, one at a time only for the low frequencies. The n wavelet decomposition of $f(x)$ can be expressed as:

$$f(x) = R_1 f + R_2 f + \cdots + R_n f + P_n f \tag{2}$$

where, $P_n f = \sum_k c_k^n \varphi_{nk}, R_n f = \sum_k d_k^n \psi_{nk}, c^j = Hc^{j-1}, d^j = Gc^{j-1}$. c^j, d^j are the approximation and detail signals of the original signal c^o at a resolution of 2^{-j}, H, G is the operator, and $P_0 f = f$.

The wavelet decomposition is performed using the Mallat algorithm, and the approximation and detail signals obtained after each decomposition are reduced by half of the number of points of the signal before decomposition, and the reduction of the number of points is detrimental to the prediction. However, the reconstruction can be performed using the reconstruction algorithm, which is:

$$\begin{aligned} P_{n-1} f &= P_n f + R_n f \\ c^{j-1} &= H^* c^j + G^* d^j \end{aligned} \tag{3}$$

where H^*, G^* is the dual operator of H, G respectively.

Suppose that the original signal f is wavelet decomposed to obtain a sequence of n approximation signals and 1 detail signal as:

$$\{s_1(m)\}, \{s_2(m)\} \cdots \{s_n(m)\}, \{u_n(m)\} \tag{4}$$

$m = 1, 2 \cdots$. Then the original signal f can be expressed as:

$$f_m = s_1(m) + s_2(m) + \cdots + s_n(m) + u_n(m) \tag{5}$$

Thus, if the value f_m of the original signal at the moment $t_m = 1, 2 \cdots n$ is known, the value f_{m+r} at the moment t_{m+r} after the r-step can be derived by summing the values of $s_1(m+r), s_2(m+r) \cdots s_n(m+r), u_n(m+r)$ obtained by the prediction of $\{s_1(m)\}, \{s_2(m)\} \cdots \{s_n(m)\}, \{u_n(m)\}$ respectively:

$$f_{m+r} = s_1(m+r) s_2(m+r) + \cdots + s_n(m+r) + u_n(m+r) \tag{6}$$

The monitoring data show that the ground temperature near the upper limit of the permafrost under the roadbed is a non-stationary time series with a clear warming trend. The reason is that the permafrost under the roadbed is the result of the combined effect of engineering and global warming. For this non-stationary time series, the approximate component sequence $\{u_n(m)\}$ and the approximate component sequence $\{s_1(m)\}\{s_2(m)\} \cdots \{s_n(m)\}$ are obtained by wavelet multilevel decomposition, which are simulated by BP neural network model and ARIMA model, respectively. After obtaining its most stable model, the wavelet decomposition prediction model for the prediction of multi-year permafrost temperature under the roadbed is established according to Eq. (3), and then the prediction is carried out according to Eq. (4).

II. D.Freeze-thaw hazard prediction based on ARIMA modeling

Smoothness tests are generally performed when ARIMA modeling is performed on time series [23]. The smoothness of time series can be categorized into two types according to their constraints: strictly smooth time series and extensively smooth time series. A strictly smooth time series is one in which all statistical properties of the time series do not change over time, while an extensively smooth time series is one that is approximately smooth as long as the lower order distance (second order) of the time series is smooth. Simply put, strict smoothness is a definition of smoothness with relatively stringent conditions. It holds that a series can be considered smooth only if all statistical properties of the series do not vary over time, whereas extensive smoothness is a type of smoothness defined using the characteristic statistics of the series. It is believed that the statistical properties of a series are mainly determined by its low-order moments. Therefore, as long as the low-order moments of the series are stable, the main properties of the series are guaranteed to be approximately stable. The general smoothness test refers to extensive smoothness, and the smoothness test methods are: plotting method, Dickey-Fowler test (DF test), Augmented Dickey-Fowler test (ADF test), PP test, and KPSS test.

The data obtained in engineering is usually non-smooth data, which is not conducive to data fitting and model construction, in the process of building ARIMA model, it usually needs differential processing to make the series data conform to the smooth state, and then modeling and forecasting. Assuming that time $\{t_n\}(n = 1, 2, 3, \cdots\cdots, n)$ corresponds to an indicator observed value of $\{x_n\}(n = 1, 2, 3, \cdots\cdots, n)$, and $\{x_1, x_2, x_3, \ldots, x_{n-1}, x_n\}$ fluctuations are

large, it is necessary to carry out differential processing and smoothness test. The difference processing method is shown in equation (7):

$$\Delta x_i = x_{i+1} - x_i (i = 1, 2, \cdots\cdots, n-1, n) \tag{7}$$

Let $y_i = \Delta x_i$, then the series $\{y_1, y_2, y_3, \ldots\ldots, y_{n+1}\}$ is called the first-order difference of the series $\{x_1, x_2, x_3, \ldots\ldots, x_{n-1}, x_n\}$, if the first-order difference still does not meet the requirements of the smoothness test, it is necessary to carry out the second-order difference, the second-order difference method is similar to the first-order difference, specifically as shown in equation (8):

$$\Delta y_i = y_{i+1} - y_i (i = 1, 2, \cdots\cdots, n-1, n) \tag{8}$$

Let $z_i = \Delta y_i$, the series $\{z_1, z_2, z_3 \ldots . z_{n-2}\}$ is known as the series $\{y_1, y_2, y_3, \ldots, y_{n-1}\}$ of the first-order difference, higher-order difference algorithm is similar to the above first- and second-order difference algorithm, and will not be described here. In addition to first- and second-order difference, there is another method of difference processing is k -step difference, for time series $\{x_n\}(n = 1, 2, 3, \cdots\cdots, n)$, k -step difference:

$$\Delta x_{ik} = x_i - x_{i-k} (i = k+1, k+2, \cdots\cdots, n) \tag{9}$$

Let $q_i = \Delta y_i$, then series $\{q_1, q_2, q_3, \cdots\cdots, q_{n-k}\}$ is called a k -step differential of series $\{x_{k+1}, x_{k+2}, x_{k+3}, \cdots\cdots x_{n-1}, x_n\}$.

II. D. 1) ARIMA model

The full name of ARIMA model is Differential Integrated Moving Average Autoregressive Model, also known as Autoregressive Differential Moving Average Model, which is a time series forecasting model developed on the basis of Autoregressive Model (AR), Moving Average Model (MA), and Autoregressive Moving Average (ARMA). In order to better illustrate and explain its principles, AR, MA, ARMA, and ARIMA models are introduced in turn.

(1) AR model: using the historical data of a variable to make predictions about itself, applicable to phenomena related to historical data, p st order autoregressive model is defined as follows:

$$x_t = \mu + \sum_{i=1}^{p} \gamma_i x_{t-i} + \varepsilon_t \tag{10}$$

where x_i is the current value, μ is the constant term, p is the regression order, γ_i is the autoregressive coefficient, and ε_i is the error. The model reflects that there is a linear relationship between the value of the target value at the t moment and the previous $t-1 \sim t-p$ target value before.

(2) MA model: the moving average model is concerned with the accumulation of the error term in the autoregressive model. The 8th order regression process is defined as follows:

$$x_t = \mu + \sum_{i=1}^{q} \theta_i \xi_{t-i} + \varepsilon_t \tag{11}$$

where x_i is the current value, μ is the constant term, q is the moving order, θ_i represents the partial autocorrelation coefficient, ξ_{i-i} is the difference between the current term x_i and the $t-i$ term x_{t-i} and ε_i is the error. The model reflects that there is a linear relationship between the target value at the t moment and the first $t-1 \sim t-q$ error value.

(3) ARMA model: a combination of autoregressive model and moving average model. The defining equation is as follows:

$$x_t = \mu + \sum_{i=1}^{p} \gamma_i y_{t-i} + \varepsilon_t + \sum_{i=1}^{q} \theta_i \xi_{t-i} \tag{12}$$

where, x_i is the current value, μ is the constant term, p is the autoregressive order, γ_i is the autoregressive coefficient, ε_i is the error, q is the order, θ_i represents the partial autocorrelation coefficient, and ξ_{t-i} is the difference between the current term x_i and the $t-i$ term x_{t-i} .

(4) ARIMA model: on the basis of the ARIMA (p,q) model in front, plus the smoothing process when the difference process, it is the ARIMA (p,d,q) model, for the difference over the sequence of ARMA modeling, it is the original sequence of ARIMA model.

II. D. 2) ARIMA modeling process

The modeling process of ARIMA model is shown in Figure 1, when the engineering data is obtained, the first smoothness test is performed, after the smoothness test, the series must be determined to be suitable for the establishment of the model category (AR, MA, ARMA, ARIMA), the model category can be determined by the model test. The model test needs to use the autocorrelation coefficient (ACF) and partial autocorrelation coefficient (PACF), so before this should be obtained ACF and PACF. determine the modeling type to determine the number of model orders, as mentioned above, common smoothness test methods are: plotting, DF test, ADF test, PP test test test and so on. Among them, DF method, ADF method, PP method is to determine whether the sequence is smooth or not by judging the presence or absence of the unit root of the sequence. In this paper, the plotting method is used to conduct the smoothness test, when the series has no obvious upward and downward trend and the fluctuation is small, it is considered that the series is a smooth series.

When the data is not smooth, it can be transformed into a smooth series after first-order differencing or second-order differencing. After transforming into a smooth series, the correlation coefficient and autocorrelation coefficient need to be obtained for model testing and order fixing.The ACF is defined as follows:

$$ACF(k) = \rho_k = \frac{cov(x_t, x_{t-k})}{var(x_t)} \tag{13}$$

The PACF is defined as follows: after eliminating the middle $k-1$ random variables, the correlation coefficient is found for the remaining series:

$$PACF(k) = \rho_{X_t, X_{t-k} | X_{t-1}, X_{t-k+1}} = \frac{cov(x_t, x_{t-k})}{var(x_t)} \tag{14}$$

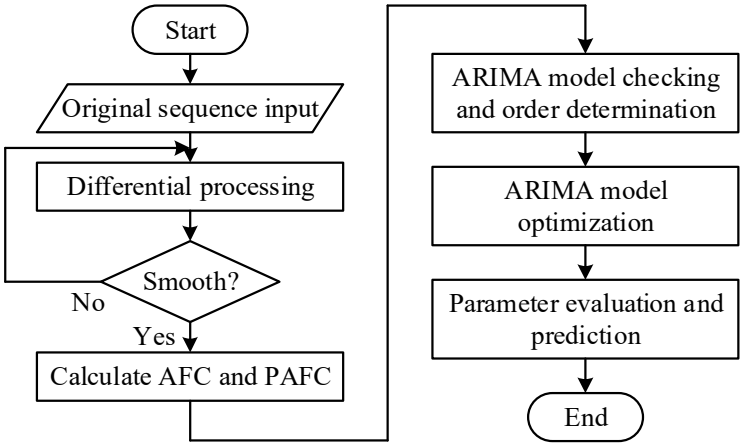

Figure 1: ARIMA Modeling Flowchart

II. E. BP Neural Network Model

II. E. 1) Network structure of BP neural networks

BP neural network is a multi-layer feed-forward neural network that utilizes nonlinear functions for weight training, and the topology of this network model includes input, hidden, and output layers. And each neuron between the upper and lower layers realizes full connection [24]. Its algorithmic learning process mainly includes two aspects, the forward propagation of input values on the one hand, and the reverse direction propagation of errors on the other. The original input data determines the number of nodes in the input and output layers of the network, but there is no uniform method for determining the number of hidden layers, which is usually calculated by empirical formulas to determine the number of nodes in the hidden layer in the BP neural network, as follows:

$$y = \sqrt{m+n} + a \tag{15}$$

II. E. 2) Mathematical Principles of BP Neural Networks

The forward propagation process is after initializing the neural network, the input signal is passed through the input layer, processed layer by layer by connecting the weights and calculating the is actual output value of each unit. Then the bias corresponding to the neurons in the hidden layer is summed and added, and finally the obtained

results are normalized. The following is illustrated by the specific formula, the input of the j st node on the hidden layer is:

$$y_i - f(\sum w_{ij}x_i + b_j) \tag{16}$$

The output of the k st node on the input layer is:

$$y_i - f(\sum w_{ij}x_i + b_j) \tag{17}$$

$$y_k = f(\sum w_{jk}y_j + b_k) \tag{18}$$

The backpropagation process starts by comparing the actual output value with the desired output value, if the desired error is not reached then the neural network weights and biases are calculated based on the gradient descent algorithm, and the values of the updated weights and biases are calculated by substituting them layer by layer. The above process is illustrated below by the formulae, the purpose of back propagation is to calculate the change in weights between individual neurons and the change in bias. The weights and biases are adjusted by the error to achieve the desired error margin. First the weights and bias are calculated between the input layer and the hidden layer. Define the incremental formula as follows:

$$\Delta w_{jk}(n) = \alpha\delta_k X_j \tag{19}$$

where δ_k is:

$$\delta_k = (d_k - Y_k)Y_k(1 - Y_k) \tag{20}$$

Then the new weight $w_{jk}(n+1)$ is obtained as.

$$w_{jk}(n+1) = \Delta w_{jk}(n) + w_{jk}(n) \tag{21}$$

The increment of the bias is obtained by the same reasoning.

$$\Delta b_{jk}(n) = \beta\delta_k \tag{22}$$

This in turn yields the bias update formula.

$$b_{jk}(n+1) = \Delta b_{jk}(n) + b_{jk}(n) \tag{23}$$

Calculate the update of weights and biases and compute the updated weights: the

$$\begin{aligned} &\Delta w_{ij}(n) = \alpha\sigma_j X_k \\ &\sigma_j = \sum \kappa\delta\kappa w_{jk} H_j(1 - H_j) \\ &w_{ij}(n+1) = \Delta wi_j(n) + w_{ij}(n) \end{aligned} \tag{24}$$

Bias Updates.

$$\begin{aligned} &\Delta bi_j(n) = \beta\sigma_j \\ &b_{ij}(n+1) = \Delta b_{ij}(n) + b_{ij}(n) \end{aligned} \tag{25}$$

In the above equation α, β is the learning rate, which defines the parameters of the BP neural network structure and defines the input variables as.

$$X_k = \left[x_{k1},\ \ x_{k2},\ \ x_{k3},\ \ \cdots,\ \ x_{kN}\right] \tag{26}$$

$k = 1, 2, \cdots, N$ is the number of training samples. Define the nth iteration network input actuals as.

$$Y_k = \left[y_{k1},\ \ y_{k2},\ \ y_{k3},\ \ \cdots,\ \ y_{kp}\right] \tag{27}$$

Define the desired output value as.

$$d_k = \left[d_{k1},\ \ d_{k2},\ \ d_{k3}\ \ \cdots,\ \ d_{kp}\right] \tag{28}$$

II. F. Freeze-thaw hazard prediction based on wavelet decomposition method

II. F. 1) Training of Predictive Models

Take the range of common roadbed layout parameters in the actual project, such as t_c take -25 ~ -28 ℃, ζ / l take 0.5 ~ 2, ζ / L take 0.5 ~ 2 and l / L take 0.5 ~ 1 for the solution, the number of roadbeds n take 1, 2, 3, respectively, represents a single row, double row and three rows, t_c, respectively, take -25 ℃ and -28 ℃, r_0, take 45, 55mm, l, respectively, 0.6, 0.8, 1, 1.2, 1.4 m. The calculation results as the training and testing data set of the neural network model, Table 1 shows the statistical results of the general prediction model based on the wavelet decomposition method, 1, 1.2, 1.4 m, and the calculation results are used as the training and testing dataset of the neural network model. Table 1 shows the statistical results of the data of the generalized prediction model based on the wavelet partitioning and solving method, where t_c is the temperature of the roadbed, r_0 is the radius of the roadbed, ζ is the thickness of the permafrost wall of half of it, l is the spacing of the roadbed, L is the spacing of the roadbed of the double rows, and n is the number of the roadbeds. Randomly selected 548 groups of data (80%) to train the network model, the other 137 groups (20%) as a test use, the allowable error is 0.001, a total of 225 iterations to meet the requirements, the average value of the roadbed temperature of -30 ° C or so.

Table 1: Statistical results of general prediction model based on small fractal solution

Parameter	Minimum value	Maximum value	Mean	Standard deviation
n	1	10	4.73	2.75
t_c /°C	-28	-25	-30	1.5
r_0 / mm	45	55	50	0
l / m	0.5	1.5	1	0.3
ζ / m	0.25	3	1.5	0.8
L / m	0	4	1.6	0.95
t_{cp} /°C	-25.65	-6.6	-20	3.95

II. F. 2) Validation of measurement models

The wavelet decomposition generalized prediction model was trained and tested based on the solved 685 sets of data, and the results of the comparison between the predicted and calculated values are shown in Fig. 2, Fig. (a) shows the comparison between the calculated values and the predicted values, and Fig. (b) shows the cumulative frequency percentage of the error percentage of the predicted values. The training and testing data have high prediction accuracy, the correlation coefficient R^2 reaches 0.98 and 0.97 respectively, and the mean square error MSE is 0.0024 and 0.0045 respectively. the cumulative frequency percentage of the data with the error percentage less than 1% accounts for about 90% of the data, which indicates that the trained model has good simulation effect on the roadbed one-lane, two-lane roadbed, and the roadbed multi-lane scenarios.

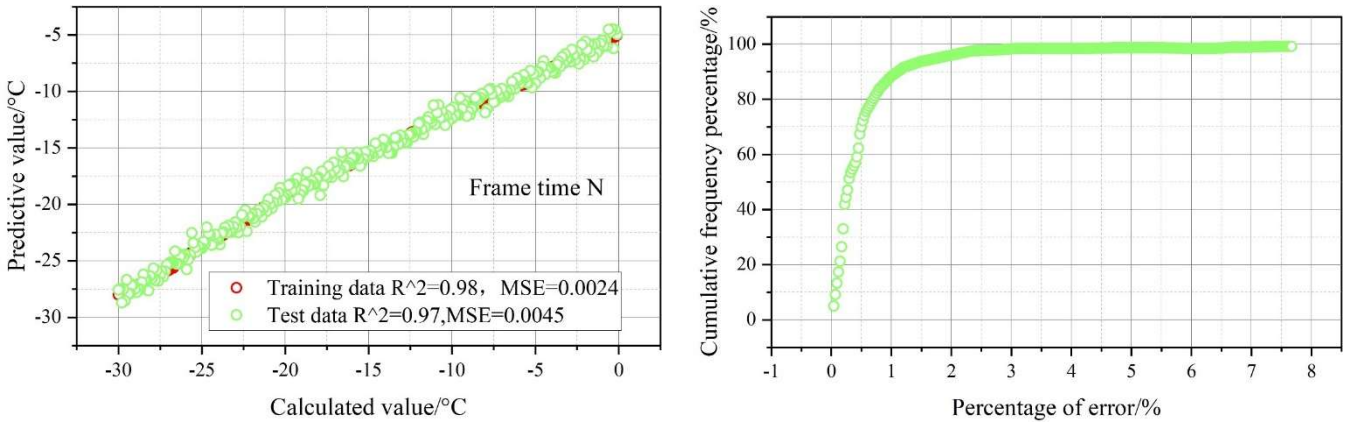

(a) The calculated value is compared to the predicted value

(b) The cumulative frequency percentage of the predicted value error percentage

Figure 2: Comparison of calculated and predicted values and error analysis

II. F. 3) Characteristics of chronological changes in roadbed temperature

Table 2 shows the multi-year average temperature of the surface temperature at representative stations on the

Tibetan Plateau, and preliminary measurements of the surface temperature of the high-speed railroad on the Tibetan Plateau were made by using the model. The increase of the surface temperature on the Tibetan Plateau is obvious, especially in the winter, from -1.5963 ℃ in the 1990s to 0.5495 ℃ in the 2020s, and the rate of warming reaches 0.336 ℃/10a, but the temperature remains stable from the 2010s to the 2020s. The warming rate is 0.336 ℃/10a, but from 2010s to 2020s, the temperature remains stable. The warming rate of the plateau surface temperature in summer is smaller than that in winter. During the warming process, there is also a cooling in the 2010s, which makes the warming from the 2010s to the 2020s appear to be very rapid. The annual average surface temperature warming rate is 0.4365°C/10a, which is faster than the average annual temperature change along the Qinghai-Tibet Railway.

Table 2: The temperature of the surface temperature for many years

Season	Year				Years average
	1990	2000	2010	2020	
Winter	-1.5963	-0.2485	0.5693	0.5495	-8.8465
Summer	-0.4956	-0.1355	-0.3485	0.7965	15.8636
Annual average	-0.5486	-0.2485	0.1685	0.7986	4.3265

III. High-speed railroad foundation engineering applications on the Qinghai-Tibetan Plateau

III. A. Temperature changes and their forecasts

III. A. 1) Inter-annual variations and trends in temperature

Figure 3 shows the interannual variation of the average temperature at Tuotuo River and Naqu Station. The highest values of the monthly average temperature at Tuotuo River and Naqu Station over the years have obvious interannual and generational variations. By comparing the interannual variations between the two stations, it can be seen that although there is a significant temperature difference of higher in the south and lower in the north between the highest values of the monthly average temperature, However, its interannual variation is relatively consistent, and its correlation coefficient is 0.75, exceeding the reliability level of 0.001. This indicates that in summer, the main body of the plateau along the Qinghai-Tibet Railway is influenced by the same climate system and has consistent interannual variation characteristics. In the study of the literature, it was found that the interannual variation of summer temperature in the central part of the Qinghai-Tibet Plateau is uniformly affected by the convergence line of the plateau. The results of this paper are consistent with it. The linear trend analysis shows that the maximum monthly average temperature values of the two stations have very close long-term variation trends, which are 0.0754℃·a^{-1} and 0.117℃·a^{-1} respectively. However, in the past 20 years, this changing trend has risen sharply, reaching 0.3722℃·a^{-1} and 0.3℃·a^{-1}, and its warming trend is very obvious.

Studying the changes of the monthly mean temperature minimum of the Totuohe and Nagqu stations in the past years, the interannual change characteristics are also obvious, but the changes between the two stations are not consistent, and the correlation analysis shows that there is no significant correlation exists between them. This suggests that in winter, the southern and northern parts of the plateau along the Qinghai-Tibet Railway are affected by different climate systems, which makes the interannual variations distinctly different. The linear trend analysis shows that the monthly mean temperature minimum at TuoTuoHe station in winter has a decreasing trend of -0.018℃-a^{-1}. From the graph, this is related to the low temperature caused by the snowstorms on the Qinghai-Tibet Plateau in 1985 and 1986, but even if this particular point is excluded, the linear trend of the long-term change is still up to -0.013℃-a^{-1}. The monthly mean temperature minimum at the Naqu station is the same as that at TuoTuoHe station. On the contrary, Naqu is a strong upward trend, and its long-term trend of 50 a is as high as 0.076℃ a^{-1}, which is mainly affected by the low temperature in the 1960s. Nearly 20 a change trend slowed down, but still up to 0.0448 ℃-a^{-1}.

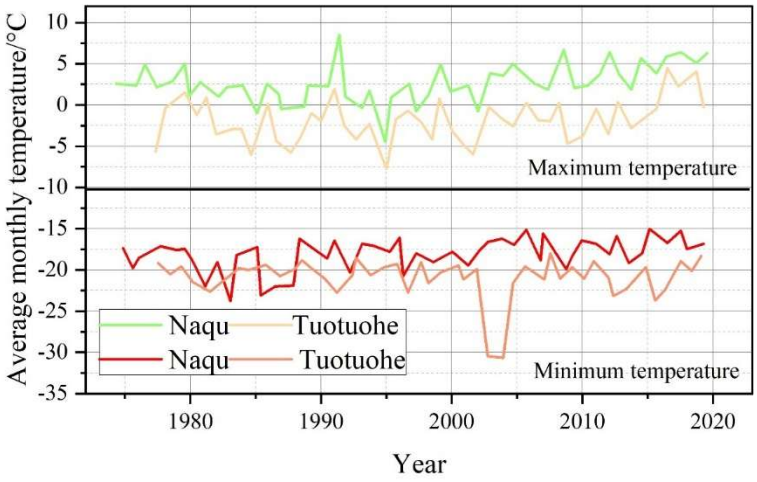

Figure 3: The max and min monthly air temperatures at Tuotuohe and Naqu Stations

III. A. 2) Projections of long-term trends in temperature change

Based on the interannual variation series of the minimum and maximum values of the monthly mean temperatures in all the years at Tuotuo and Naqu stations, the original series was processed by ARIMA model to predict the minimum and maximum values of the monthly mean temperatures in 2020.

Firstly, the original series was decomposed into the long-term change trend term and the fluctuation change term, and then the fluctuation series with the removal of the long-term change trend was reconciled and analyzed to obtain the significance period, which was selected here as 2019. n, is the length of the episodic time period. The two episodic series are synthesized to obtain the prediction series, and the average of the last 10a, i.e., 2010-2019, is taken as the prediction of the 2010s, and the prediction results of the minimum and maximum values of the monthly mean temperature at TuoTuoHe and NaQu stations are shown in Table 3.

In 2020, the highest predicted monthly average temperature at TuoTuoHe and NaQu stations will be 8.4652℃ and 9.7685℃ respectively, an increase of 0.5707℃ and 0.2196℃ over 2000. The lowest predicted value of the monthly mean temperature at the Totuohe station is -17.8996℃, a decrease of 0.5514℃ compared with that of 2000, and the lowest predicted value of the monthly mean temperature at the Naqu station is -12.7986℃, an increase of 0.0656℃ compared with that of 2000s. This indicates that the overall trend of the prediction is reasonable.

Table 3: Prediction of the lowest and highest values of the monthly average temperature

/	Tuotuohe Average monthly temperature	
	Maximum value	Minimum value
2000 Measured	7.8945	-17.3482
2020 Prediction	8.4652	-17.8996
Predict change	0.5707	-0.5514
/	Naqu Average monthly temperature	
	Maximum value	Minimum value
2000 Measured	9.5489	-12.8642
2020 Prediction	9.7685	-12.7986
Predict change	0.2196	0.0656

III. B. Prediction of roadbed surface temperature and thaw index

III. B. 1) Prediction of roadbed surface temperatures

Table 4 shows the melting and freezing indices and the freeze-thaw ratio of the temperature at the TuoTuoHe and Naju stations. From the predicted melting and freezing of the temperature at the TuoTuoHe and Naju stations in the 2020s, there is a clear trend towards melting. Compared with the 2000s, the increase in the melting index at the Totuohe station is larger, more than 10% or more, and although the freezing index has increased by nearly 2.51%, the rise in the freeze-thaw ratio is still larger, at about 8%. The increase of melting index of Naqu station is smaller, about 2.8%, but because of its freezing index is decreasing, so it makes the thawing ratio increase, and the increase of thawing ratio value is slightly larger than that of TuoTuo river, although because of its thawing ratio is

larger than that of the base so that its increase is not as large as that of TuoTuo river station, but it is also in the range of about 4.82%.

Table 4: The temperature melting index, freezing index and the ratio of melting to freezing

/	Tuotuohe			Tuotuohe		
	Melt index /(°C·d)	Freezing index /(°C·d)	Frost ratio	Melt index /(°C·d)	Freezing index /(°C·d)	Frost ratio
2000 Measured	695	-2428	-0.28624	1015	-1625	-0.62462
2020 Prediction	769	-2489	-0.30896	1043	-1593	-0.65474
Predict change	74	-61	0.022716	28	-32	0.030124

Since the original model is designed to be used for the calculation of the instantaneous values of specific times, the predicted values of the roadbed surface temperatures of 24 times throughout the day are first calculated according to the daily changes in air temperature and then averaged, and the results are shown in Table 5. In addition to the TuoTuo river winter monthly average roadbed surface temperature minimum value slightly decreased (<0.1 ℃), TuoTuo river and NaQu area roadbed surface temperature in the 2020s predicted value than the measured value of the 2000s have increased significantly, and the rate of increase is larger. Among them, TuoTuo river area is the summer roadbed surface temperature rise is larger, the rise reached 0.7501 ℃, while the Naqu area is the winter roadbed surface temperature rise is larger, the rise reached 0.5521 ℃, and the temperature listed in Table 3 predicted changes can be seen, the summer roadbed surface temperature rise is close to the temperature, TuoTuo river summer roadbed surface temperature rise is larger because of the temperature rise caused by the large. Winter Tuotuo River and Naqu roadbed surface temperature are much higher than the air temperature, and Tuotuo River roadbed surface temperature rise partially offset the decline in air temperature, so that the predicted change in roadbed surface temperature is only a slight decrease.

Table 5: The surface temperature of the subgrade is the highest and lowest

/	Tuotuohe/°C		Naqu°C	
	Maximum value	Minimum value	Maximum value	Minimum value
2000 Measured	14.4985	-16.8968	15.3469	-11.3486
2020 Prediction	15.2486	-16.9548	15.5486	-10.7965
Predict change	0.7501	-0.058	0.2017	0.5521
Surface temperature direct extrapolation	16	-20	15.6	-10

III. B. 2) Prediction of Freezing and Thawing Index of the Roadbed Surface

Table 6 shows the prediction of roadbed surface freezing and thawing index, except for the Tuo Tuo River roadbed surface freezing index predicted change is not obvious (<1%), other values have a large variation. Compared with 2000, in 2020, TuoTuo river summer roadbed surface thawing index increased significantly, winter freezing index slightly reduced, so that its thaw-thaw ratio has a large increase in the predicted thaw-thaw ratio of more than 7%, reaching 0.8473. Thaw-thaw ratio is still maintained below 1, indicating that its freezing capacity is still predominant, but its advantage has been in the obvious weakening, that is, the perennial permafrost in the degradation of the direction of development! Because of the lower latitude and stronger sunshine in the Nagqu area, the warming in winter and summer is more obvious, the melting index of the roadbed surface increases while the freezing index decreases, which makes the thaw-frost ratio jump substantially, and the predicted thaw-frost ratio rises by more than 10% or more, reaching 1.7768. In short, compared with the year 2000, there is a clear tendency for the roadbed permafrost in TuoTuoHua and the Nagqu area to develop in the direction of thaw-frost in the year 2020. As a comparison, the last row in Table 6 gives the thawing index of the roadbed surface calculated from the thawing index of the predicted temperatures using the n coefficient method. The n-coefficient is calculated from the measured values in 2000. It can be seen that the thaw index obtained by the n-coefficient method is closer to the model calculation.

Table 6: Prediction of roadbed surface freeze and thaw index

/	Tuotuohe			Tuotuohe		
	Melt index /(°C·d)	Freezing index /(°C·d)	Frost ratio	Melt index /(°C·d)	Freezing index /(°C·d)	Frost ratio
2000 Measured	1600	-2035	0.78624	1930	-1195	1.61506
2020 Prediction	1715	-2024	0.84733	1990	-1120	1.77679
Predict change	115	11	0.061091	60	75	0.161723
N Coefficient method	1709	-1930	0.885492	2018	-1160	1.739655

IV. Conclusion

The study constructed a risk prediction model for freezing and thawing disaster of roadbed of high-speed railroad on the Qinghai-Tibetan Plateau, and predicted and analyzed the freezing and thawing condition of roadbed in the Qinghai-Tibetan Plateau region, and drew the following conclusions:

The roadbed freeze-thaw disaster risk prediction model constructed based on wavelet decomposition, ARIMA and BP neural network methods has high prediction accuracy, with correlation coefficients R^2 reaching 0.98 and 0.97, respectively, and the cumulative frequency of the data with an error percentage of less than 1% is about 90%, which indicates that the model has good simulation effect for the roadbed one-way, two-way and multi-way schemes.

The temperature of the Tibetan Plateau shows an obvious rising trend, and the maximum monthly mean temperature at TuoTuoHe and NaQu stations has reached 0.3722℃·a^{-1} and 0.3℃·a^{-1} respectively in the recent 20-year warming trend, and the predicted 2020 TuoTuoHe and NaQu station monthly mean temperature of 2020 are 8.4652℃ and 9.7685℃ respectively, which are 0.5707℃ and 0.2196℃ higher than that of 2000.

The frozen soil condition of the roadbed in the Tibetan Plateau region is developing in the direction of thawing, and it is predicted that in 2020, the surface thawing index of the roadbed in the Nagqu region will be 1990℃·d, the freezing index will be -1120℃·d, and the thawing ratio will reach 1.7768, which is over 10% higher than that of 2000; and the predicted thawing ratio of the roadbed surface in the Totuohe region will be 0.8473, up more than 7% from 2000.

Under the background of global warming, the risk of freezing and thawing disaster of the roadbed of the high-speed railroad on the Qinghai-Tibet Plateau will continue to increase, and it is recommended to take full consideration of the rising temperature and the trend of permafrost degradation in engineering design and maintenance, and to take corresponding roadbed reinforcement and protection measures.

Funding

This work was supported by National Natural Science Foundation of China (Grant No.: 12462022).

References

[1] Luo, L., Duan, Q., Wang, L., Zhao, W., & Zhuang, Y. (2020). Increased human pressures on the alpine ecosystem along the Qinghai-Tibet Railway. Regional Environmental Change, 20(1), 33.

[2] Zhang, L., Miao, Y., Wei, H., & Dai, T. (2023). Ecological Impacts Associated with the Qinghai–Tibet Railway and Its Influencing Factors: A Comparison Study on Diversified Research Units. International Journal of Environmental Research and Public Health, 20(5), 4154.

[3] Liu, H., Huang, S., Xie, C., Tian, B., Chen, M., & Chang, Z. (2023). Monitoring Roadbed stability in permafrost area of Qinghai–Tibet railway by MT-InSAR technology. Land, 12(2), 474.

[4] Niu, F., Lin, Z., Lu, J., Liu, H., & Xu, Z. Y. (2011). Characteristics of roadbed settlement in embankment–bridge transition section along the Qinghai-Tibet Railway in permafrost regions. Cold Regions Science and Technology, 65(3), 437-445.

[5] Ma, Q., Lan, T., Lai, Y., Luo, X., & He, P. (2024). Application of the cooling measures in the highway roadbed in permafrost regions of the Qinghai-Tibet Plateau. Cold Regions Science and Technology, 221, 104177.

[6] Chen, K., Li, G., Su, F., Lu, J., Dong, T., Zhao, Y., & Yu, Q. (2024). Deformation causes of the Embankment-Bridge transition section in warm permafrost: The case study of a dry bridge along the Qinghai-Tibet railway. Engineering Failure Analysis, 163, 108476.

[7] Zhdanova, S., & Neratova, O. (2020). Complex solutions for providing roadbed stability on permafrost. In Transportation Soil Engineering in Cold Regions, Volume 1: Proceedings of TRANSOILCOLD 2019 (pp. 233-241). Singapore: Springer Singapore.

[8] Ye, W., & Li, C. (2019). The consequences of changes in the structure of loess as a result of cyclic freezing and thawing. Bulletin of Engineering Geology and the Environment, 78, 2125-2138.

[9] Zhou, F., Xie, S., Wang, L., Ma, Z., Zhou, P., Jiang, Y., ... & Wang, Z. (2024). Disaster Mechanism and Frost Heave Effect of Railway Tunnel Induced by Drainage System Failure in High Latitude Cold Region. KSCE Journal of Civil Engineering, 28(10), 4190-4213.

[10] Liu, N., Yang, Y., Li, N., Liang, S., Liu, H., & Li, C. (2024). The stability issue of fractured rock mass slope under the influences of freeze–thaw cycle. Scientific Reports, 14(1), 5674.

[11] Li, J., Wang, F., Yi, F., Wu, F., Liu, J., & Lin, Z. (2019). Effect of freeze-thaw cycles on triaxial strength property damage to cement improved aeolian sand (CIAS). Materials, 12(17), 2801.

[12] Cui, K., Wu, G., Du, Y., An, X., & Wang, Z. (2019). The coupling effects of freeze-thaw cycles and salinization due to snowfall on the rammed earth used in historical freeze-thaw cycles relics in northwest China. Cold Regions Science and Technology, 160, 288-299.

[13] Chen, H., Gao, X., & Wang, Q. (2023). Research progress and prospect of frozen soil engineering disasters. Cold Regions Science and Technology, 212, 103901.
[14] Feng, X. Z., & Liu, Z. P. (2012). Discussion on permafrost hazards of railway engineering and prevention measures: a case study on Qinghai-Tibet railway. Advanced Materials Research, 550, 2493-2497.
[15] Cui, P., Zou, Q., Wang, J., You, Y., Chen, X., Chen, H., ... & Su, F. (2022). Landslide Risk Along the Sichuan-Tibetan Railway. Impact of Climate Change, Land Use and Land Cover, and Socio-economic Dynamics on Landslides, 83-121.
[16] Li, Z., Wang, W., Xu, L., & Peng, B. (2024). Long-term freeze–thaw cycle behavior of high-speed railway embankment in frozen soil regions and its effects on train-track dynamic interaction system. Transportation Geotechnics, 46, 101237.
[17] Xie, H., Xu, L., & Yan, B. (2023). Mechanical Properties of Ballastless Track Considering Freeze–Thaw Deterioration Damage. Mathematics, 11(10), 2289.
[18] Xu, X., Du, X., & Wu, W. (2024). Triggering Mechanism and Mitigation Strategies of Freeze-Thaw Landslides for Engineering in Cold Regions: A Review. Recent Geotechnical Research at BOKU, 265-282.
[19] Lu, F., & Si, W. (2024). Reliability risk modelling of asphalt pavement structure performance under the impact of freeze-thaw cycles. Case Studies in Construction Materials, 20, e03054.
[20] Zhou, C., Chen, M., Chen, J., Chen, Y., & Chen, W. (2024). A Multi-Hazard Risk Assessment Model for a Road Network Based on Neural Networks and Fuzzy Comprehensive Evaluation. Sustainability, 16(6), 2429.
[21] Xuebing Zhang,Jia Wang,Zhizhan Chen,Yang Quan,Zhizhou Zheng,Tianyun Zhang... & Ping Xiang. (2025). A distributed fiber optic sensor-based approach for crack asphalt structure under freeze-thaw cycling tests. Construction and Building Materials,476,141262-141262.
[22] W. Chabeh & A. Saoudi. (2025). Multidimensional continuous Bessel wavelet transform: properties and applications. Integral Transforms and Special Functions,36(5),348-370.
[23] Spyridon Karamolegkos & Dimitrios E. Koulouriotis. (2025). Advancing short-term load forecasting with decomposed Fourier ARIMA: A case study on the Greek energy market. Energy,325,135854-135854.
[24] Xiaodong Zhang,Yiquan Li,Peng Yu,Yongcheng Gao & Sijun Dong. (2025). Prediction of microgroove performance indicators based on BP neural network in micro-EDM. Materials Today Communications,46,112465-112465.